metals

MDPI

Article

Advancing Wire Arc Directed Energy Deposition: Analyzing Impact of Materials and Parameters on Bead Shape

Stephen Price [1,*], Kiran Judd [2], Matthew Gleason [2], Kyle Tsaknopoulos [2], Danielle L. Cote [2] and Rodica Neamtu [1]

[1] Department of Computer Science, Worcester Polytechnic Institute, Worcester, MA 01609, USA; rneamtu@wpi.edu
[2] Department of Mechanical and Materials Engineering, Worcester Polytechnic Institute, Worcester, MA 01609, USA; kgjudd@wpi.edu (K.J.); magleason@wpi.edu (M.G.); kltsaknopoulos@wpi.edu (K.T.)
* Correspondence: sprice@wpi.edu

Abstract: This study advances foundational knowledge regarding the impact of processing parameters and material selection on bead shape in Wire Arc directed energy deposition (Wire Arc DED) additive manufacturing. Through the collection and analysis of the largest Wire Arc DED bead shape dataset to date, this work confirms the dominant roles of the feed rate and travel speed on bead shape. Specifically, an increasing feed rate correlates with an increased bead size, while increasing the travel speed decreases the bead size. Furthermore, as the first dataset to directly compare bead shape across different wire–substrate combinations, this research identified that material selection has a smaller, but still relevant, impact on bead shape compared to the feed rate and travel speed. These insights into the roles of parameters and materials are critical for improving large-scale manufacturing efficiency and quality with Wire Arc DED. By generating a robust, multi-material dataset, this work enables applications of machine learning to optimize Wire Arc DED through quicker manufacturing, reduced material waste, and improved structural integrity.

Keywords: wire arc DED; bead geometry; bead shape; characterization; optimization; welding

check for updates

Citation: Price, S.; Judd, K.; Gleason, M.; Tsaknopoulos, K.; Cote, D.L.; Neamtu, R. Advancing Wire Arc Directed Energy Deposition: Analyzing Impact of Materials and Parameters on Bead Shape. *Metals* **2024**, *14*, 282. https://doi.org/10.3390/met14030282

Academic Editor: Jafar Razmi

Received: 30 January 2024
Revised: 23 February 2024
Accepted: 26 February 2024
Published: 28 February 2024

Copyright: © 2024 by the authors. Licensee MDPI, Basel, Switzerland. This article is an open access article distributed under the terms and conditions of the Creative Commons Attribution (CC BY) license (https://creativecommons.org/licenses/by/4.0/).

1. Introduction

The U.S. Navy is currently seeking to increase the production of submarines and surface ships [1]. However, the manufacturing process includes an extensive development and certification process for casts and molds, which must be repeated each time designs are updated or replaced. This extensive process, paired with an often unstable supply chain, has impeded the ability to maintain and grow the existing naval fleet [2]. Specifically, as suppliers have closed or downsized, the original molds no longer exist, making it challenging to fabricate replacement parts [1]. Wire arc directed energy deposition (Wire Arc DED), an additive manufacturing (AM) technique using an electric arc to melt and deposit metal layer-by-layer, has presented itself as a potential solution to this problem [3]. With the capability to manufacture parts with less material waste, increased design flexibility, rapid prototyping [4], and its higher deposition rate, material utilization, and energy efficiency [5,6], research dedicated to Wire Arc DED manufacturing has grown in recent years [7]. Instead of needing to store casts or molds, Wire Arc DED utilizes CAD files and robot path planning [8], eliminating the need to store and maintain large casts or molds. Furthermore, without needing to create casts, prototyping can be made more efficient by enabling more-rapid refinement, lowering overhead costs, and improving sustainability [9]. As part of a larger initiative evaluating the efficacy of replacing traditional manufacturing with Wire Arc DED, this work seeks to explain and highlight the relationship between the materials, processing parameters, and the resultant bead shape (width and height) of single-layer prints.

To the best of our knowledge, this is the largest collected dataset relating processing parameters to bead shape. As articulated in Wu et al. (2018) [10], a pressing demand exists for analyzing the influence of material selection on the characteristic properties of Wire Arc DED. To address this, the impact of material selection and parameter selection was evaluated by utilizing multiple wire and substrate materials during the dataset-collection process. Additionally, characterization was extended beyond the width and height of beads to include the width variance and height variance, measuring the consistency of a bead's geometry. Throughout this process, a robust and standardized approach was developed to extract bead geometries under various circumstances, thereby improving the precision and consistency of the measured results.

With this dataset, this research aims to analyze the intricate relationship between various materials and processing parameters in Wire Arc DED. This will allow prevailing trends to be confirmed across different materials and enable the determination of whether specific alloys magnify or suppress specific trends. Moreover, critical insights for material selection in Wire Arc DED can be obtained by evaluating the impact of different materials under consistent processing conditions, uncovering material-specific influences on the bead shape. Accurate predictions of weld bead shape and geometry significantly enhance the efficiency and quality of manufacturing large-scale AM components. Furthermore, the ability to accurately model, optimize, and predict the weld bead geometry is critical to achieving consistently high-quality, high-strength welded joints and deposits [11–13].

Contributions

Ultimately, this work offers the following contributions:

1. Introduces a novel design of experiment (DOE) to enhance variability and reduce required samples when designing datasets for modeling purposes.
2. Collects and explores, to the best of our knowledge, the largest dataset relating Wire Arc DED parameters to bead shape, enabling more-sophisticated analysis and modeling techniques.
3. Performs, to the best of our knowledge, the first direct comparison of Wire Arc DED bead shape across multiple wire–substrate material combinations, facilitating deeper understandings and more-generalizable results.
4. Outlines a novel standardized methodology to extract bead geometries from printed parts, ensuring consistent measurements regardless of thermal expansion.
5. Extends bead geometry characterization to also consider the variability of a given bead's geometry, allowing researchers to optimize the consistency of prints.

2. Background

2.1. Wire Arc DED Processing

Current AM techniques can be broken into two main categories: powder-feed/bed or wire-feed processing [14]. In the past, AM research was primarily dedicated to studying and improving powder/bed processing due to its ability to develop parts with a high geometric accuracy [5]. However, in recent years, research dedicated to wire-feed AM has increased due to its higher potential material utilization (up to 100%), higher deposition rate (up to 330 g/min for stainless steel) [5], and growing ability to print complex geometries, as shown in Figure 1.

Wire-feed processing techniques have three distinct sub-fields: laser, electron-beam, and welding-arc. Each uses a unique energy source to melt and layer the wire component. Compared to laser and electron-beam techniques, Wire Arc DED (utilizing a welding-arc) has lower equipment expenses, a higher material deposition efficiency, and a more-environmentally friendly production process [6]. Additionally, Wire Arc DED has a higher energy efficiency (90%) compared to laser (2–5%) and electron-beam (15–20%), allowing for the fabrication of large-scale parts with lower production costs and time [15]. Despite the increasing focus on Wire Arc DED technology, much remains to be discovered and analyzed, including a deeper understanding of material and parameter selection [10].

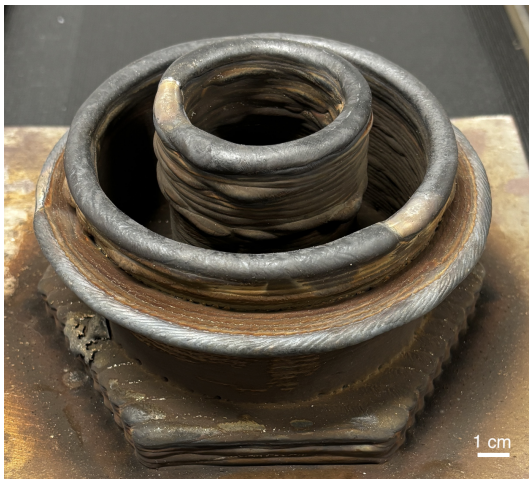


Figure 1. Pre-machined WA-DED sample highlighting the complex geometries available.

When using Wire Arc DED manufacturing, the initial printing phase yields a larger piece with rough edges, as shown in Figure 1, which must be refined to the desired part. The efficiency of this refinement process is dependent on the processing parameters chosen. An optimal set of parameters minimizes the material wasted and time consumed, whereas a suboptimal set of parameters can result in significant waste from oversized structures requiring extensive machining. As a result, suboptimal parameters lead to wasted material, increased costs, and slowed production. To remedy this, when a new project is initiated, a series of single-layer test prints (referred to as beads) are printed in search of the desired quality and tolerances, as shown in Figure 2.

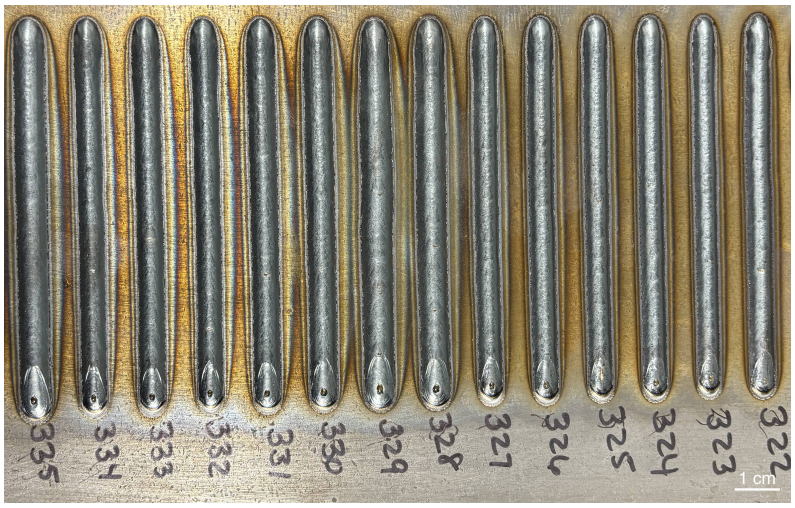
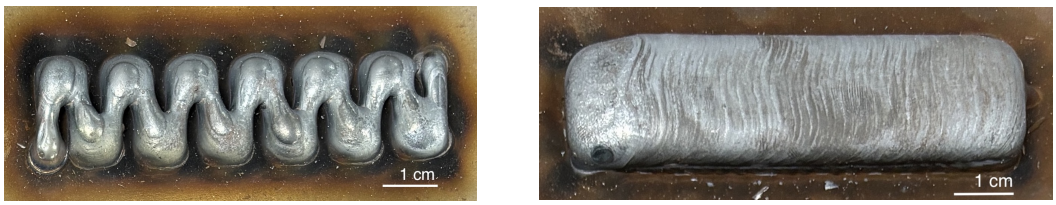


Figure 2. A series of Wire Arc DED test prints, referred to as beads, to evaluate the impact of processing parameters on the deposited material.

2.2. Impacts of Informed Path Planning

In addition to optimizing material usage and reducing waste, printing test beads allows researchers to define a well-informed path plan for the robotic arm that deposits material. In particular, these beads can be measured to identify the standard width and height of the deposited material, which can be used to calculate how closely the layers of the deposited material should be to each other [16]. Beads that are printed too far apart cause porous sections or gaps to form in the material, as shown in Figure 3a, which compromises the structural integrity of the manufactured parts. However, when the layers of the deposited material are printed an appropriate distance from each other, they bond together, forming a uniform deposit, as shown in Figure 3b. To achieve this optimal path

planning, such as the one shown in Figure 3b, researchers must know the width and height of the deposited material, requiring test beads, as shown in Figure 2.



(**a**) (**b**)

Figure 3. Visual example of the impact a well-designed path plan has on the deposited material. (**a**) Deposited material with poor path planning, where runs are spaced too far apart, causing gaps. (**b**) Deposited material with good path planning, where runs are close enough to ensure uniform bonding.

At an extreme, too large of a distance between deposits can cause holes in manufactured parts. In less-severe cases, when the deposited material is too far apart, a phenomenon called height error can occur in which two beads bond to fill a wider space and, as a result, are less tall [16]. As more layers are printed, the height of the deposited material continues to diverge from the expected height, which can result in the arc losing contact with the deposited material, halting production.

Ultimately, knowledge of the relationship between processing parameters and the resultant bead shape is not only useful for the optimization of material waste, but also critical for the structural integrity and completion of a manufactured part. Thus, test prints are utilized at the start of each project, especially when a new material is introduced. However, collecting these data is quite expensive. In this study, each bead cost approximately USD 13, and considering the 13,000+ parameter combinations given the chosen materials, it would have cost over USD 150,000 to collect a complete dataset. Given these constraints, a smaller dataset was collected. While not performed here, this dataset was designed to enable machine learning to predict the remaining conditions that were not collected. For example, it was collected with explicit training and test splits for an impartial model performance evaluation. Additionally, while the specific samples collected were pseudo-random to prevent bias, the dataset was balanced so that the trained models would be representative and unbiased.

3. Methods

Acquiring a dataset to analyze the impact of materials and processing parameters on bead geometry required multiple distinct steps. Since collecting every parameter combination was too costly and time-consuming, a selection process was performed to decide which parameter combinations should be evaluated. This process used pseudo-randomness to select parameter combinations and reduce bias while ensuring that the resultant dataset remained balanced. Once complete, a 6-inch-long, single-layered metal bead was printed for each of the selected parameter combinations. These beads were then scanned with an optical scanner to digitize their structural makeup, allowing their dimensions to be calculated.

3.1. Design of Experiment

This work analyzes the impact of four input parameters (wire material, substrate material, wire feed rate, and travel speed) on the resultant bead's shape (width and height). For the evaluation, there were 40 options for the wire feed rate and 17 for the travel speed, in addition to five selected wire compositions and four selected substrate compositions, as shown in Table 1. Exhaustively collecting every parameter combination would require 13,940 samples (41 wire feed rates $\times$ 17 travel speeds $\times$ 5 wires $\times$ 4 substrates), which our facilities could not accommodate.

Table 1. Summary of available values for each parameter to analyze resultant bead shape from Wire Arc DED manufacturing. Note: wire and substrate materials were selected from these corresponding lists, but could not be incremented by a specific value.

Parameter	Range of Values	Increment
Wire Material	308LSi; L-50; L-56; LA-75; LA-90	NA
Substrate Material	304 SS; 4140; A572; low carbon	NA
Wire Feed Rate	200–400 in/min	5 in/min
Travel Speed	80–160 mm/s	5 mm/s

A common solution to reduce the number of samples needed within material science is a factorial design of experiment (DOE) [17]. However, a factorial design can decrease the variability of entries, causing repeated values within a given feature. As a result, trends could only be identified at specific intervals, potentially leading to missing information on what was occurring between these intervals.

Additionally, using machine learning on this dataset in the future could result in less-precise models due to these intervals. To mitigate these effects, a novel DOE was implemented, which used a modified factorial approach using bins of multiple values instead of repeating specific values. In this DOE, each feature's parameter values were discretized into bins (e.g., low, medium, high). Combinatorial sampling generated a parameter set for every unique bin combination. For example, one sample consisted of all low bins and another of all low bins, except one medium, and this incrementally varied the bin used for each feature. Once the bin combinations had been established, a value was randomly selected from each sample's assigned bins.

This sampling was performed to encompass the full range of processing parameters with fewer repeated values. By selecting from a range of values within a bin instead of using the same value every time, variability was introduced into the dataset, enabling improved model performance and generalizability for future machine learning models. While pseudo-randomly selecting values introduced variability into the dataset, constraining selection to bins ensured the resultant dataset remained balanced with the same number of entries per bin, as shown in Figure 4. However, even though the distribution per bin was guaranteed to be balanced, the distribution of values within a given bin were not for two main reasons. First, the number of unique values within a feature may not be perfectly divisible by the number of bins, as was the case for the feed rate and travel speed. As a result, one of the bins had fewer values, causing the values in this bin to be selected more frequently. Second, due to the inherent random nature of the generation process, some values were repeated more frequently, leaving others less frequent. Figures 5 and 6 highlight this phenomenon, in which Figures 5 and 6 were both perfectly balanced at the bin level. Despite being balanced at the bin level, the number of occurrences of each individual value in Figure 6 was visibly less balanced than Figure 5. To quantify this difference, in the more-balanced dataset, as shown in Figure 5, the number of occurrences of a given value in the feed rate occurred between 8 and 17 times, a range of 9 occurrences. In contrast, for the less-balanced use case, the number of occurrences varied from 4 to 24, with a range of 20 occurrences.

Since distributions like Figure 5 are equally as likely as Figure 6, a method was required to ensure that the generated dataset was closer to a distribution like Figure 5 than Figure 6. Thus, a procedure was required to evaluate and compare the generated datasets to determine which one exhibited the most balance at the value level. To accomplish this, an algorithm was developed to evaluate a generated dataset and assign a numeric quality score. This was achieved by calculating the number of expected entries per distinct value by dividing the number of distinct values by the number of entries. This was then compared against the actual number of entries per value, calculating the RMSE, which was then divided by the expected number of entries per value, giving the percent error for the individual feature. This error was then averaged across every feature to compute the final score of the generated dataset. With these algorithms, 15,000 datasets were generated and evaluated to select the one with the lowest error to be collected.

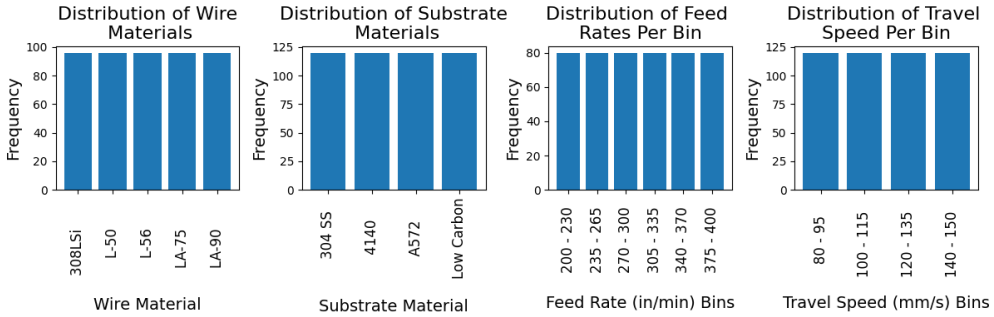


Figure 4. Distributions of values per bin per feature, highlighting the balanced nature of a designed experiment.

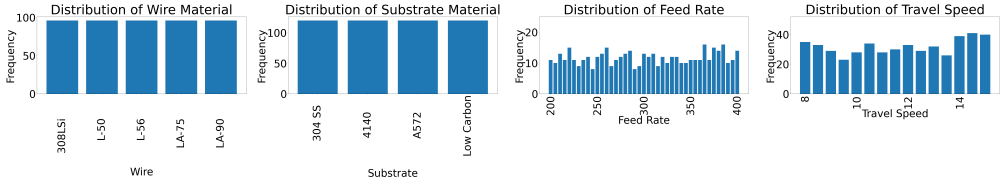


Figure 5. A relatively evenly balanced distribution of values.

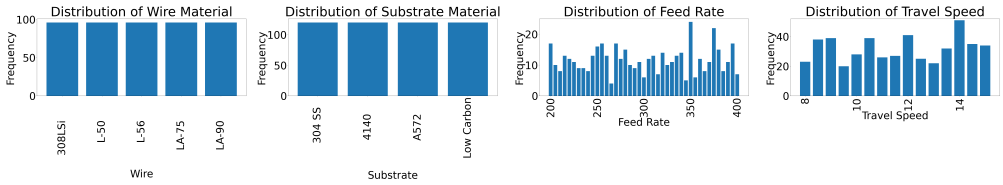


Figure 6. A less-evenly balanced distribution of values.

Using this technique, two datasets were generated, creating a training set with 480 samples and a test set with 96 samples to serve as external validation for any trained models. Any entry in the validation set that also occurred in the training set was replaced with a similar sample comprised of the same bins, but different feature values within those bins. These two datasets were generated before collecting any data so any models trained and evaluated had an impartial evaluation without data leakage, implicitly or accidentally [18]. Using this novel proposed DOE, the dataset was designed with a reduced number of Wire Arc DED parameter combinations while ensuring that the dataset was expansive of all ranges of values. Additionally, through the inserted randomness, this dataset was more-continuous, filling gaps between discrete intervals that would occur if a factorial approach were performed, making it suitable for future machine learning projects.

3.2. Printing Parameter Combinations

After the dataset was designed, the parameter combinations were printed for evaluation using a Fronius TPS400i welder (Fronius, Pettenbach, Austria) with an ABB IRB 2600 robot (ABB Ltd. , Zürich, Switzerland) and a gas mixture of 98% argon and 2% CO_2. Instead of maintaining a constant current and voltage, a specialized technique called "cold metal transfer" was implemented. This approach, developed by Fronius, uses a modified short-circuit welding process to synchronize the waveform with the mechanical motion of the wire. This process contributes to a controlled and precise material deposition during the additive manufacturing process.

Generated vs. Experimentally Collected Dataset

Due to the large size, weight, and costs of steel required to collect this dataset, all of the materials required were sourced at the start of this project. Initially, it was anticipated that 30 parameter combinations could be evaluated on each substrate plate. However,

during the material deposition phase, it was discovered that some of the beads were larger than anticipated and required more space between each test to prevent corrupting the results. This adjustment reduced the maximum number of beads per plate to 28 or 29. As a result of this adjustment, the available materials were depleted prior to evaluating every combination. While the original dataset design aimed for 576 samples, 480 for a training set and 96 for testing, the experimentally obtained dataset comprised 553 samples, with 461 for training and 92 for testing, accounting for approximately 96% of the initially planned dataset. Since the missing samples represented a very small portion of the dataset and were distributed across all of the materials, it was decided to proceed with the analysis.

3.3. Three-Dimensional Scanning of Printed Beads

Once printing each parameter combination was completed, an Artec Space Spider 3D Scanner (Artec 3D, San Diego, CA, USA) was used to measure each bead. This high-resolution 3D scanner utilizes structured blue light technology to capture and render complex geometric shapes. This scanner is specifically designed for quality and control engineering and is ideal for small objects with intricate detail, as was the case here. The 3D scanner automatically saved all scans using an A3D file format. While this format is common for 3D models, it was difficult to extract the necessary information from it. The 3D models were converted to Standard Triangle Language (STL) files, a more-common file type that was easier to work with. STL files are made up of a collection of points that form a mesh of connected triangles to model the shape of an object. Once converted, it was possible to extract the necessary information from these STL files. However, due to the structure of interwoven triangles forming a mesh, this would require quite a bit of processing. As a result, a surface metrology software called MountainsMap 9.1 from DigitalSurf (Besançon, France)was used to extract and analyze surfaces. This software enabled us to analyze the surfaces of each plate. Additionally, using MountainsMap, the surface of each 3D model was represented as a point cloud matrix with constant sampling in the X and Y direction at 0.25 mm intervals, which made it much simpler to extract the desired target variables from.

3.4. Calculating Target Variables from Extracted Surfaces

To calculate each bead's width and height, a two-step process was performed. First, the width and height were calculated at a specific cross-sectional view. Then, these measurements were aggregated over all of the cross-sectional views for a comprehensive width and height measurement of the bead.

3.4.1. Calculating Width and Height from Cross-Section

With plates scanned and surfaces extracted, as shown in Figure 7, extracting the widths and heights required identifying local extrema (minimums and maximums). However, this process was challenging for three main reasons. First, the plates on which the beads were printed were physically warped due to the heat input during the printing, as shown in Figures 8 and 9. Second, the magnitude and shape of each plate's curve was inconsistent. As shown in Figures 8 and 9, the plate represented by Figure 8 has a steeper, binomial curve, whereas the plate represented by Figure 9 has a shallower, cubic curve. Lastly, since these plates were measured with a precision of 0.0001 µms in the Z direction, they were not very smooth, creating local extrema, which did not represent the peak or base of the bead.

Due to these challenges, a naive solution identifying changes in direction was often insufficient and led to overestimations of bead width and height, particularly on the edges of plates, where the curvature was most significant, as shown in Figure 10a. To address this, a more-complex algorithm capable of adapting to various magnitudes and shapes of curvature was developed. This enhanced algorithm also considered the plate's slope in addition to just changes in direction for a more-accurate identification of where the beads intersected with the plate. This was accomplished by making an initial estimate on which measured values corresponded to a bead and which corresponded to the plate. Focusing solely on measurements associated with the plate, the algorithm computed an equation

representing the plate's curvature. To identify which local maxima correspond with the peak of beads, this equation was offset by a value close to, but less than the smallest bead's height. Any local maxima above this offset equation must correspond to a bead, whereas any below must be noise and were filtered out. Each bead's left and right base points were then determined by locating the points of convergence between the line's slope and the base plate's equation on either side of the maxima. As shown in Figure 10b, with these modifications, the algorithm more precisely and consistently measured the geometry of a bead, regardless of where on the curve it is located.

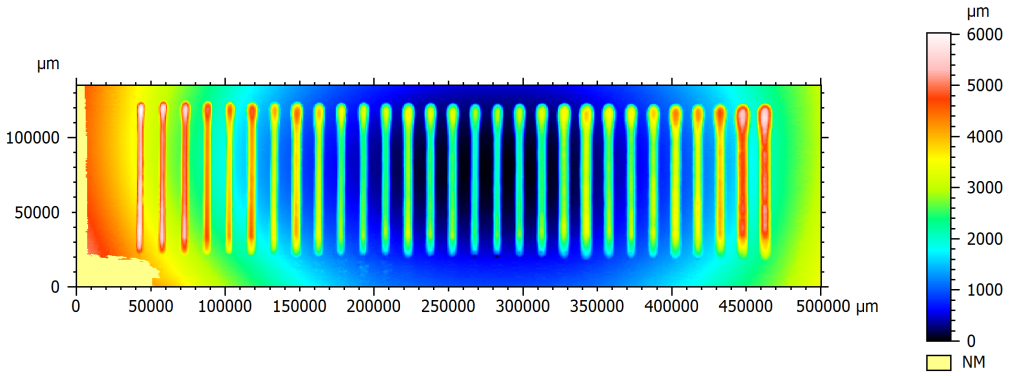


Figure 7. Surface profile of low-carbon steel plate with 29 beads printed with SuperArc LA-90 wire (Bead IDs 30 to 58).

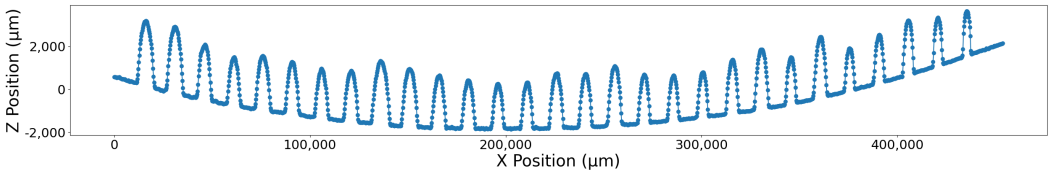


Figure 8. An example of a binomial curvature of the substrate plate due to thermal expansion during the manufacturing process.

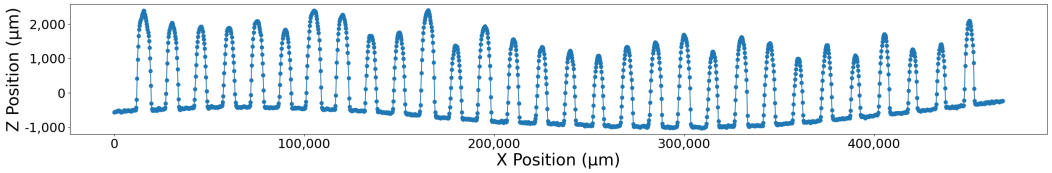


Figure 9. An example of a cubic curvature of the substrate plate due to thermal expansion during the manufacturing process.



(**a**) (**b**)

Figure 10. Improved extrema detection for calculating width and height by including the slope in consideration. (**a**) Issues from naive solution of identifying base points of beads due to curve. (**b**) Improved solution to identify base points of beads using the slope.

With the location of the peak and base points identified, calculating the width and height of each bead became quite simple. The height was calculated as the distance from the Y-value of the peak to the average Y-value of the two base points. The width was calculated as the Pythagorean distance from the two base points so the plate's curvature did not affect the results.

3.4.2. Joining Multiple Cross-Sectional Views Together

While some previous works have calculated the width and height using a single cross-section [19], a larger section of the bead was used here for a more-accurate measurement. Thus, once the width and height could be calculated for a single cross-sectional view, these results were aggregated over the whole bead. However, to prevent the plate, starting point, or finishing point of the bead from impacting the results, only the middle 50% of the cross-sections were aggregated, maximizing the number of cross-sectional views included while still ensuring a clean measurement. The final width and height values were calculated as the mean value of each cross-sectional measurement for the middle 50% of each scan, which was usually about 170 unique measurements, but varied slightly. Additionally, the width variance and height variance were calculated as the standard deviation of these measurements across the middle 50% of each bead.

4. Results and Discussion

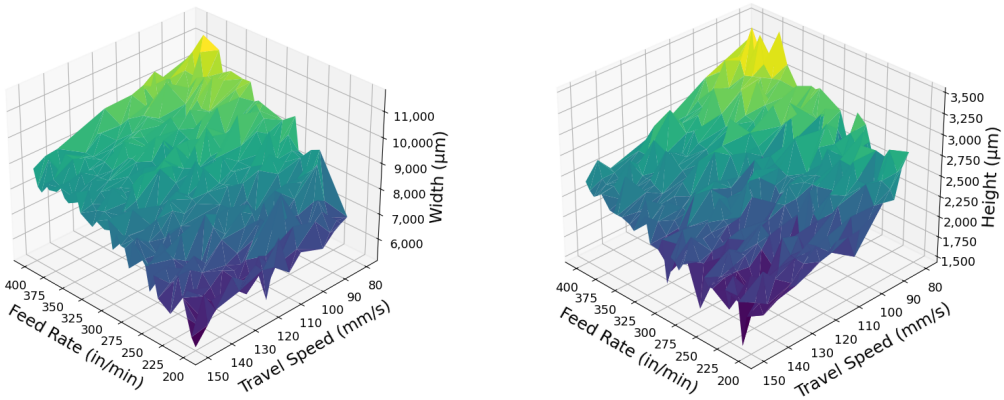
Once the 553 parameter combinations had been printed, scanned, and processed, the data were analyzed to identify trends within the data. To accomplish this, a visual inspection was carried out, target variables were graphed against the input features, and correlation matrices were calculated. After analyzing all of the data, a machine learning model was trained to evaluate how well these data could be predicted. As a result of these insights, future manufacturing procedures can be optimized to achieve faster and higher-quality prints.

4.1. Relating Feed Rate and Travel Speed to Bead Geometry

Previous studies have indicated a negative relationship between travel speed and width and positive relationships between feed rate and height [20]. These conclusions were confirmed by plotting the feed rate and travel speed with respect to the width and height, as shown in Figure 11. These graphs revealed that the width and height were both positively related to the feed rate and both negatively related to the travel speed, confirming and extending the conclusions of Dinovitezer et al. [20]. Comparing the width, as shown in Figure 11a, to the height, as shown in Figure 11b, the height had a linear relationship with both parameters, forming a relatively straight hyperplane. In contrast, the width appeared to have a non-linear, but still monotonic, relationship with the feed rate and travel speed, forming a more curved surface. The 3D contour plots, as shown in Figure 11, were plotted using all of the collected data, which included four substrates and five wires. This inclusion of multiple materials is likely the cause of the rough surfaces shown. Despite these variations in material, there was still a clear and visible trend, confirming that the feed rate and travel speed were more relevant to the bead shape than the material selection.

4.2. Analyzing Correlations Between Features and Target Variables

In addition to the visual analysis of specific features such as feed rate and travel speed, the linear and non-linear correlations of the independent and dependent variables were analyzed. To accomplish this, a Pearson correlation matrix was used for the linear correlations, as shown in Figure 12 and a Spearman correlation matrix was used for the non-linear correlations, as shown in Figure 13. This study calculates and includes correlations between all collected variables. However, due to the designed nature of the dataset, the primary focus was on the correlations with the dependent variables, namely width, height, width variance, and height variance.



(**a**) (**b**)

Figure 11. Contour maps relating processing parameters feed rate and travel speed to target variables width and height. (**a**) Relating feed rate and travel speed to bead width. (**b**) Relating feed rate and travel speed to bead height.

The analysis of the linear correlations between the input features and target variables confirmed the conclusions reached by Dinovitzer et al. [20] and from the visual analysis in Section 4.1 of this study. As found by Dinovitzer et al. [20], bead width was negatively associated with travel speed (−0.49 out of −1), while bead height was positively correlated with feed rate (0.55 out of 1). Further examination revealed that bead width had an even stronger positive correlation with feed rate (0.78) than bead height (0.55), and bead height had an even stronger negative correlation with travel speed (−0.71) than bead width (−0.49). Evaluating the impact of the feed rate on all dependent variables showed positive correlations with width (0.78), height (0.55), and height variance (0.49), but a negative correlation with width variance (−0.30). In contrast, there was no correlation between travel speed and width variance (0.05) and only a small correlation with height variance (−0.10). In addition to the impact of feed rate and travel speed, correlations between materials were also identified, indicating an impact on geometry. For example, BlueBax 308LSi had a positive correlation with width variance (0.23), whereas SupeArc L56 had a negative correlation (−0.15). This would indicate that, while feed rate and travel speed are the most-important factors impacting bead geometry, the material is also relevant and must be considered.

Having already analyzed the linear correlations, the focus of the evaluation of the non-linear correlations was primarily on the changes from linear to non-linear trends. Thus, the difference was analyzed, as shown in Figure 13, where a positive value indicates a stronger non-linear relationship and a negative value indicates a weaker non-linear relationship than its linear counterpart. Interestingly, this identified that the linear and non-linear correlations from width and height to the processing parameters were always quite similar, never deviating by more than 0.03. In contrast, larger deviations between the linear and non-linear correlations of width variance and height variance indicated a stronger non-linear relationship. As a result, attempting to control or optimize the width variance and height variance of the Wire Arc DED bead shape would likely be more complicated than for width and height.

4.3. Impact of Parameters as Combinations of Materials' Change

In addition to measuring the pairwise correlation between individual processing parameters and materials on bead geometry, the impact of inter-correlated features was also evaluated. Specifically, an analysis was performed to identify how changing the wire and substrate material impacted the correlation between travel speed and feed rate on width, height, width variance, and height variance, as shown in Figure 14. Based on

these results, it was concluded that there was an interrelated nature between materials and processing parameters and how they impacted bead geometry. For example, while feed rate had a consistent positive correlation with width, the magnitude of this correlation varied. Looking at beads deposited on A572 steel substrates, depending on the wire used, this correlation ranged from 0.64 (Super Arc L50) to 0.84 (Super Arc La-56). In contrast, when using 304 stainless steel for the substrate, this separation was much tighter, ranging from 0.79 to 0.88. However, in some cases, a change of material did not only impact the closeness of the values, but actually inverted them. For example, when using the Super Arc LA-90 wire, there was a linear correlation between the feed rate and width variance of -0.36, -0.55, and -0.24 for the 4140, low carbon, and A572 substrates, respectively. However, when using the same wire on 304 stainless steel, the correlation was $+0.58$, a significant shift from the other substrates, which was not observed with the other wires.

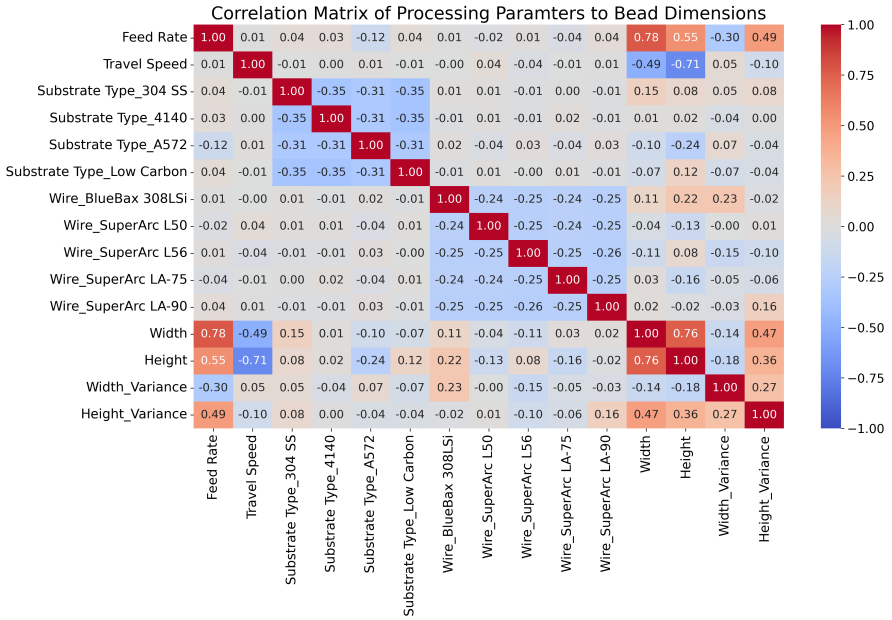


Figure 12. Pearson correlation matrix identifying linear correlations between features.

This analysis confirmed that, while the feed rate and travel speed are the most-relevant factors impacting bead shape, the material must be considered when predicting or seeking to understand bead shape. Thus, future works will seek to analyze if there are discernible traits about each material, whether chemical or physical, to quantify and model how specific materials impact bead geometry. Additionally, analyzing this data broken down by material showed width and height had small changes due to the material used, but width variance and height variance were much more susceptible to change. This could be the case for a few different reasons including width variance and height variance being more impacted by factors that were not measured or potentially have a degree of randomness to them, which this dataset was not large enough to capture. Further research is required to identify this.

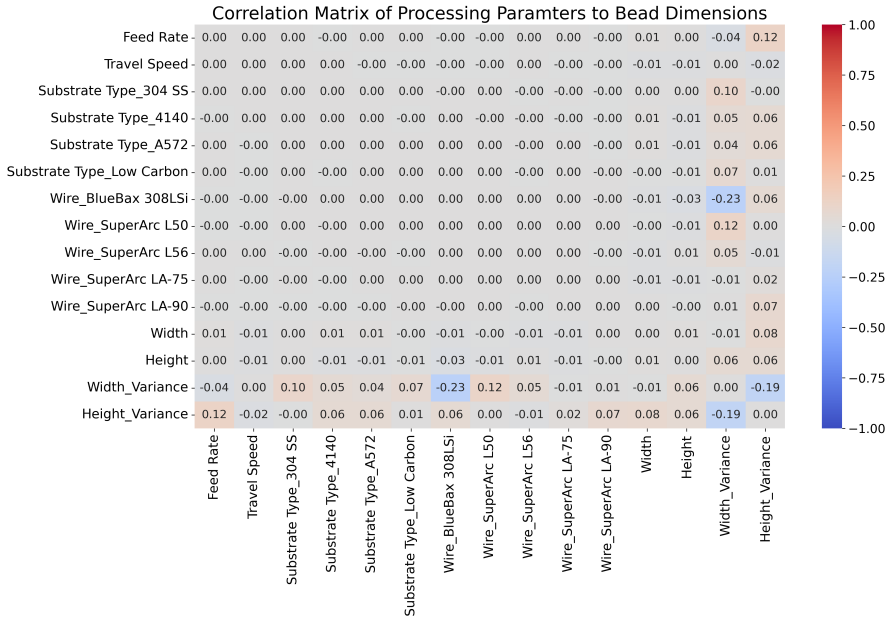


Figure 13. Difference from Spearman correlation matrix and Pearson correlation matrix with a positive number indicating a stronger non-linear correlation and a negative number indicating a stronger linear correlation.

		4140		Low Carbon		304 SS		A572	
		Travel Speed	Feed Rate	Travel Speed	Feed Rate	Travel Speed	Feed Rate	Travel Speed	Feed Rate
Super Arc La-90	Width	-0.55	0.70	-0.44	0.86	-0.46	0.85	-0.39	0.82
	Height	-0.73	0.58	-0.88	0.42	-0.85	0.49	-0.74	0.58
	Width Variance	0.03	-0.36	0.00	-0.55	-0.18	0.58	0.31	-0.24
	Height Variance	-0.22	0.65	0.33	0.77	-0.21	0.73	-0.15	0.61
Super Arc La-56	Width	-0.48	0.80	-0.39	0.82	-0.43	0.85	-0.52	0.84
	Height	-0.79	0.59	-0.86	0.35	-0.83	0.54	-0.92	0.37
	Width Variance	0.02	0.20	-0.25	-0.77	-0.30	-0.27	-0.04	0.23
	Height Variance	-0.19	0.71	0.11	0.62	-0.16	0.42	-0.07	0.25
SuperArc LA-75	Width	-0.49	0.76	-0.44	0.88	-0.49	0.82	-0.73	0.69
	Height	-0.74	0.57	-0.82	0.56	-0.77	0.62	-0.90	0.50
	Width Variance	0.17	0.25	0.42	-0.28	-0.27	0.06	0.08	0.35
	Height Variance	-0.26	0.75	-0.11	0.84	-0.34	0.64	-0.76	0.47
SuperArc L50	Width	-0.58	0.72	-0.62	0.80	-0.39	0.88	-0.65	0.64
	Height	-0.78	0.61	-0.85	0.55	-0.74	0.66	-0.93	0.24
	Width Variance	0.22	-0.51	-0.13	-0.22	-0.02	-0.59	-0.06	-0.33
	Height Variance	-0.23	0.71	0.13	0.70	-0.26	0.88	-0.36	0.58
BlueBax 308LSi	Width	-0.61	0.76	-0.71	0.74	-0.59	0.79	-0.70	0.72
	Height	-0.75	0.68	-0.84	0.61	-0.73	0.71	-0.87	0.61
	Width Variance	0.34	-0.74	0.25	-0.70	0.20	-0.64	0.05	-0.81
	Height Variance	-0.10	0.77	0.10	0.54	-0.22	0.74	0.06	-0.62

Figure 14. Impact of feed rate and travel speed on width, height, width variance and height variance based on wire and substrate material.

4.4. Implications of Optimized Bead Shape Geometry

The quality of welded joints and components is influenced by various conditions that must be controlled such as the weld bead shape, geometry, and dilution [11]. An optimal balance between welding parameters and dilution between the weld filler and base materials is required to ensure the desired dimensions, strength, and corrosion resistance are obtained. Consistent and optimized weld bead profiles are essential to achieve full fusion between the base metal and filler material, minimizing defects such as undercutting and porosity within the welded joint. The geometry of weld beads, specifically the weld width, is a critical parameter that determines the weld quality and integrity [11,12,21,22]. Weld bead width plays an important role in the resultant mechanical properties and geometric fitness [11,21,23]. From a weld solidification perspective, the weld bead width affects the molten mixing of metals, heat transfer rates, and solidification patterns during welding [12]. An overly narrow bead width risks the lack of fusion defects from incom-

plete penetration, while one that is excessively wide increases residual heat, leading to greater distortion and potential cracking [22]. The optimal bead width should be as small as possible, balancing adequate penetration and fusion without overheating or sacrificing mechanical strength [22]. Furthermore, controlling factors such as travel speed, arc voltage, wire feed rate, electrode angle, and position is key to depositing a weld bead width and profile that achieves the targeted strength and ductility based on the predicted microstructure and phases formed during solidification [12,13,24]. Thus, extracting profile data and understanding the control of weld bead geometry was an essential aspect of the analysis provided in this study. Post-deposition measurements of the bead profile, along with computational models that correlate bead geometry to welding parameters, enable the optimization of welding methods to obtain consistent and high-quality welds. This is significant for performance-critical structures in naval applications, where safety and reliability hinge on consistent welds meeting stringent quality standards.

4.5. Applications for Machine Learning Purposes

This study utilizes statistical methods to analyze trends between materials, processing parameters, and Wire Arc DED geometry. However, this dataset was collected in a specific way such that future works could use it as a benchmark dataset for machine learning. In particular, it was ensured that the dataset was balanced and included variability for improved model performance. Additionally, this dataset consists of two partitions, training and test, which contain no overlap for an unbiased evaluation of the model's performance. Other studies have demonstrated that machine learning can be used to model bead shape effectively. Our goal is that these added characteristics to the dataset and its significantly larger size than others will yield more-precise models using these data. Additionally, due to the multiple wire and substrate materials included, models trained on this dataset will be the first models capable of generalizing across multiple materials when predicting bead shape. To test this, a Random Forest model was trained to evaluate the efficacy of this dataset for machine learning purposes. This model performed reasonably well, scoring an RMSE of 403.67 µms and an R^2 of 0.887 for width, as well as an RMSE of 135.88 µms and an R^2 of 0.874 for height. Without any tuning or other advanced machine learning techniques performed, these scores demonstrate that this research and the collected data are well suited for applying machine learning models. Moving forward, we plan to explore this in depth, evaluating various model architectures and applying machine learning techniques to improve model performance. With a well-trained model, we can optimize the manufacturing conditions of Wire Arc DED without requiring a time-consuming and expensive test period for new projects.

5. Conclusions

This study advances foundational knowledge regarding the impact of processing parameters and material on Wire Arc DED manufacturing. Specifically, this work has identified the dominant impact of feed rate and travel speed on bead shape, with a positive correlation between feed rate and bead shape and a negative correlation between travel speed and bead shape. Additionally, this work is the first to analyze the impact of material selection on bead shape, identifying a lower, but still relevant, impact than feed rate or travel speed. This insight is crucial for refining the efficiency and quality of additive manufacturing on a large scale. Additionally, by collecting the largest dataset and the first dataset to include distinct material combinations to date, this study will enable more-advanced applications of machine learning. Moving forward, we will use machine learning to optimize Wire Arc DED processes to improve manufacturing efficiency, material utilization, and sustainability.

Author Contributions: Conceptualization: S.P., K.T., D.L.C. and R.N.; data collection and curation: S.P. and M.G.; software: S.P.; analysis: S.P., K.J., M.G., K.T., D.L.C. and R.N.; writing: S.P., K.J., M.G., K.T., D.L.C. and R.N.; supervision: K.T., D.L.C. and R.N. All authors have read and agreed to the published version of the manuscript.

Funding: This research received no external funding.

Data Availability Statement: The raw data supporting the conclusions of this article will be made available by the authors on request.

Conflicts of Interest: The authors declare no conflicts of interest.

References

1. Cote, D. Development and Transition of HY80 Steel for Qualification to NAVSEA WIRE-DED Tech Pub. America Makes Project Call: SWAAHT: 2022; unpublished. Available online: https://www.americamakes.us/projects/5540-002-development-transition-of-hy80-steel-for-qualification-to-navsea-wire-ded-tech-pub/ (accessed on 25 February 2024).
2. Taşdemir, A.; Nohut, S. An overview of Wire Arc additive manufacturing (WAAM) in shipbuilding industry. *Ships Offshore Struct.* **2021**, *16*, 797–814. [CrossRef]
3. Ferreira, I.A.; Oliveira, J.; Antonissen, J.; Carvalho, H. Assessing the impact of fusion-based additive manufacturing technologies on green supply chain management performance. *J. Manuf. Technol. Manag.* **2023**, *34*, 187–211. [CrossRef]
4. Nie, Y.; Zhang, P.; Wu, X.; Li, G.; Yan, H.; Yu, Z. Rapid prototyping of 4043 Al-alloy parts by cold metal transfer. *Sci. Technol. Weld. Join.* **2018**, *23*, 527–535. [CrossRef]
5. Ding, D.; Pan, Z.; Cuiuri, D.; Li, H. Wire-feed additive manufacturing of metal components: Technologies, developments and future interests. *Int. J. Adv. Manuf. Technol.* **2015**, *81*, 465–481. [CrossRef]
6. Xia, C.; Pan, Z.; Polden, J.; Li, H.; Xu, Y.; Chen, S.; Zhang, Y. A review on Wire Arc additive manufacturing: Monitoring, control and a framework of automated system. *J. Manuf. Syst.* **2020**, *57*, 31–45. [CrossRef]
7. Rodrigues, T.A.; Duarte, V.; Miranda, R.; Santos, T.G.; Oliveira, J. Current status and perspectives on wire and arc additive manufacturing (WAAM). *Materials* **2019**, *12*, 1121. [CrossRef] [PubMed]
8. Busachi, A.; Erkoyuncu, J.; Colegrove, P.; Martina, F.; Ding, J. Designing a WAAM based manufacturing system for defence applications. *Procedia Cirp* **2015**, *37*, 48–53. [CrossRef]
9. Pusateri, V.; Olsen, S.; Hauschild, M.; Kara, S. Potential for absolute sustainability of Wire-Arc Additive Manufacturing: A boat propellers case. *CIRP Ann.* **2023**, *7*, 29–32. [CrossRef]
10. Wu, B.; Pan, Z.; Ding, D.; Cuiuri, D.; Li, H.; Xu, J.; Norrish, J. A review of the Wire Arc additive manufacturing of metals: properties, defects and quality improvement. *J. Manuf. Process.* **2018**, *35*, 127–139. [CrossRef]
11. Palani, P.; Murugan, N. Optimization of weld bead geometry for stainless steel claddings deposited by FCAW. *J. Mater. Process. Technol.* **2007**, *190*, 291–299. [CrossRef]
12. Murugan, N.; Gunaraj, V. Prediction and control of weld bead geometry and shape relationships in submerged arc welding of pipes. *J. Mater. Process. Technol.* **2005**, *168*, 478–487. [CrossRef]
13. Kumar, A.; Maji, K. Selection of process parameters for near-net shape deposition in wire arc additive manufacturing by genetic algorithm. *J. Mater. Eng. Perform.* **2020**, *29*, 3334–3352. [CrossRef]
14. Frazier, W.E. Metal additive manufacturing: A review. *J. Mater. Eng. Perform.* **2014**, *23*, 1917–1928. [CrossRef]
15. Xia, C.; Pan, Z.; Polden, J.; Li, H.; Xu, Y.; Chen, S. Modelling and prediction of surface roughness in Wire Arc additive manufacturing using machine learning. *J. Intell. Manuf.* **2022**, 33, 1467–1482. [CrossRef]
16. Song, G.H.; Lee, C.M.; Kim, D.H. Investigation of path planning to reduce height errors of intersection parts in wire-Arc Additive manufacturing. *Materials* **2021**, *14*, 6477. [CrossRef] [PubMed]
17. Choudhury, I.; El-Baradie, M. Surface roughness prediction in the turning of high-strength steel by factorial design of experiments. *J. Mater. Process. Technol.* **1997**, *67*, 55–61. [CrossRef]
18. Papadimitriou, P.; Garcia-Molina, H. Data leakage detection. *IEEE Trans. Knowl. Data Eng.* **2010**, *23*, 51–63. [CrossRef]
19. Xiong, J.; Zhang, G.; Hu, J.; Wu, L. Bead geometry prediction for robotic GMAW-based rapid manufacturing through a neural network and a second-order regression analysis. *J. Intell. Manuf.* **2014**, *25*, 157–163. [CrossRef]
20. Dinovitzer, M.; Chen, X.; Laliberte, J.; Huang, X.; Frei, H. Effect of wire and arc additive manufacturing (WAAM) process parameters on bead geometry and microstructure. *Addit. Manuf.* **2019**, *26*, 138–146. [CrossRef]
21. Kang, M.; Kim, Y.; Ahn, S.; Rhee, S. Spatter rate estimation in the short circuit transfer region of GMAW. *Weld. J.* **2003**, *82*, 238–247.
22. Sharma, A.; Verma, D.K.; Arora, N. A scheme of comprehensive assessment of weld bead geometry. *Int. J. Adv. Manuf. Technol.* **2016**, *82*, 1507–1515. [CrossRef]
23. Juang, S.; Tarng, Y. Process parameter selection for optimizing the weld pool geometry in the tungsten inert gas welding of stainless steel. *J. Mater. Process. Technol.* **2002**, *122*, 33–37. [CrossRef]
24. Kapil, A.; Suga, T.; Tanaka, M.; Sharma, A. Towards hybrid laser-arc based directed energy deposition: Understanding bead formation through mathematical modeling for additive manufacturing. *J. Manuf. Process.* **2022**, *76*, 457–474. [CrossRef]

Disclaimer/Publisher's Note: The statements, opinions and data contained in all publications are solely those of the individual author(s) and contributor(s) and not of MDPI and/or the editor(s). MDPI and/or the editor(s) disclaim responsibility for any injury to people or property resulting from any ideas, methods, instructions or products referred to in the content.